GeoChip-based analysis of metabolic diversity of microbial communities at the Juan de Fuca Ridge hydrothermal vent

Fengping Wang[a,1,2], Huaiyang Zhou[b,1], Jun Meng[c,1], Xiaotong Peng[b], Lijing Jiang[a], Ping Sun[c], Chuanlun Zhang[d], Joy D. Van Nostrand[e], Ye Deng[e], Zhili He[e], Liyou Wu[e], Jizhong Zhou[e,3], and Xiang Xiao[a,2,3]

[a]Key Laboratory of Marine Biogenetic Resources, Third Institute of Oceanography, State Oceanic Administration, Xiamen 361005, People's Republic of China; [b]Department of Marine and Earth Sciences, Tongji University, Shanghai 200092, People's Republic of China; [c]School of Life Sciences, Xiamen University, Xiamen 361005, People's Republic of China; [d]Department of Marine Sciences, University of Georgia, Athens, GA 30602; and [e]Institute for Environmental Genomics, Department of Botany and Microbiology, University of Oklahoma, Norman, OK 73019

Edited by David M. Karl, University of Hawaii, Honolulu, HI, and approved January 13, 2009 (received for review October 17, 2008)

Deep-sea hydrothermal vents are one of the most unique and fascinating ecosystems on Earth. Although phylogenetic diversity of vent communities has been extensively examined, their physiological diversity is poorly understood. In this study, a GeoChip-based, high-throughput metagenomics technology revealed dramatic differences in microbial metabolic functions in a newly grown protochimney (inner section, Proto-I; outer section, Proto-O) and the outer section of a mature chimney (4143-1) at the Juan de Fuca Ridge. Very limited numbers of functional genes were detected in Proto-I (113 genes), whereas much higher numbers of genes were detected in Proto-O (504 genes) and 4143-1 (5,414 genes). Microbial functional genes/populations in Proto-O and Proto-I were substantially different (around 1% common genes), suggesting a rapid change in the microbial community composition during the growth of the chimney. Previously retrieved *cbbL* and *cbbM* genes involved in the Calvin Benson Bassham (CBB) cycle from deep-sea hydrothermal vents were predominant in Proto-O and 4143-1, whereas photosynthetic green-like *cbbL* genes were the major components in Proto-I. In addition, genes involved in methanogenesis, aerobic and anaerobic methane oxidation (e.g., ANME1 and ANME2), nitrification, denitrification, sulfate reduction, degradation of complex carbon substrates, and metal resistance were also detected. Clone libraries supported the GeoChip results but were less effective than the microarray in delineating microbial populations of low biomass. Overall, these results suggest that the hydrothermal microbial communities are metabolically and physiologically highly diverse, and the communities appear to be undergoing rapid dynamic succession and adaptation in response to the steep temperature and chemical gradients across the chimney.

metagenomics | microarrays | chimney | deep sea | dynamic

Since the discovery of deep-sea (>2000 m) hydrothermal vents in 1977 (1), studies of the biological systems surrounding the vent environments have greatly expanded our knowledge of life forms on Earth. These environments provide unique models for understanding living strategies in extreme environments and for exploring questions regarding the origins and limits of life on this planet or the potential for extraterrestrial life (2, 3). The base of the deep-sea life pyramid in the vent environments consists of chemolithoautotrophic microorganisms, which are fueled by geochemical energy, such as H_2S and H_2. The vent chimney, formed by chemical interactions between the hot fluids and cold sea water, has steep chemical and thermal gradients, which provide a wide range of microhabitats for microorganisms (4, 5). Recent studies have demonstrated that microbial diversity varied from vent to vent and from days to years within the same vent field (6, 7). The unique mineralogical and chemical compositions of a chimney in the early stages of its formation may support a distinct pioneering microbial community (8, 9). By analyzing the conserved specific functional genes (such as *nifH* and *mcrA*), the metabolic diversity of some specific organisms in the mature chimneys was partially investigated (10, 11). However, because of a lack of appropriate detection technologies, the metabolic diversity and dynamics of whole-microbial communities in primitive and mature chimneys have not been examined.

Recently, high-throughput genomics technologies have shown the great potential to reveal the driving forces of evolution and how ecosystems originate in different geological settings (12). Among these advanced technologies, the microarray-based, high-throughput technologies, such as GeoChip (13), are enabling microbial ecologists to address complex ecological hypotheses at the community-wide scale (14). The GeoChip contains tens of thousands of functional gene markers so that many microbial populations and functional groups can be simultaneously detected at the whole community-wide scale. This unique capability provides incomparable insight into the spatial distribution patterns of many individual functional genes in the same sample sets. Here, we report the metabolic diversity and dynamics of the deep-sea hydrothermal vent chimneys in the Endeavour Segment of Juan de Fuca Ridge by using combined molecular approaches, including microarray hybridization, quantitative real-time PCR, 16S rRNA gene, and functional gene libraries. Our GeoChip study demonstrated that the hydrothermal microbial communities are metabolically and physiologically highly diverse, and the communities appear to be undergoing rapid dynamic succession and adaptation in response to the steep temperature and chemical gradients across the chimney.

Results and Discussion

Sample Description. During the expedition of the Alvin/Atlantis to the Juan de Fuca Ridge in 2006, we placed a cone-shaped cap on the top of a small chimney (Alvin dive no. 4243), which was vigorously venting at about 310 °C (Fig. S1). The hot fluid vented directly through the central opening of the cap, and a protochimney was observed to form on the top of the cap a few days later. This protochimney was named Proto-O, and the anhydrite and sulfide minerals formed inside the cap were referred to as Proto-I. The

Author contributions: F.W., H.Z., J.Z., and X.X. designed research; F.W., H.Z., J.M., X.P., and J.D.V.N. performed research; H.Z., Y.D., Z.H., and J.Z. contributed new reagents/analytic tools; F.W., J.M., L.J., P.S., C.Z., J.D.V.N., L.W., J.Z., and X.X. analyzed data; and F.W., C.Z., J.Z., and X.X. wrote the paper.

The authors declare no conflict of interest.

This article is a PNAS Direct Submission.

[1]F.W., H.Z., and J.M. contributed equally to this work.

[2]Present address: School of Life Sciences and Biotechnology, Shanghai Jiaotong University, Shanghai 200240, People's Republic of China.

[3]To whom correspondence may be addressed. E-mail: jzhou@ou.edu or xxwfp@public.xm.fj.cn.

This article contains supporting information online at www.pnas.org/cgi/content/full/0810418106/DCSupplemental.

Proto-O represented the newly formed porous chimney that has continuous interaction with the cold seawater, whereas the Proto-I may represent the more pristine sulfate and sulfide structures that lack intense interaction with sea water because of the protection of the cap. The protochimney was allowed to grow for 15 days before being collected for this study.

Proto-O and Proto-I are mainly composed of euhedral anhydrite (>90% in volume) by X-ray diffraction and microscopic observation of thin sections. Anhydrite is a highly porous mineral and reflects the first stage in sulfide chimney development (5). The mature chimney rock 4143-1 was from the outer part of a venting chimney from the Mothra Field and was characterized by a predominance of Zn sulfide minerals, such as wurtzite and sphalerite. These minerals commonly indicate the late stages of chimney development (5).

Quantitative PCR and Clone Libraries of 16S rRNA Genes in the Mature Chimney. Proto-O and Proto-I had an extremely low biomass, as demonstrated by very low concentrations of DNA (5–10 ng/g). The mature chimney rock 4143-1, however, had DNA concentrations up to 200 ng/g. The microbial community structure in the chimney samples was examined by 16S rRNA gene analysis. Unfortunately, no PCR products were obtained from the Proto-I and Proto-O samples, even though several different pairs of PCR primers for Bacteria and Archaea were used. This may be due to the extremely low amounts of biomass in these 2 samples.

PCR amplification of 16S rRNA gene could be achieved easily with the mature chimney 4143-1. The abundance of microorganisms in this sample was estimated to be 4.6×10^9 16S rRNA gene copies per gram (wet weight) for Bacteria, and about 10^4 copies per gram (wet weight) for Archaea by quantitative PCR, demonstrating that the detected bacterial abundance was significantly greater than Archaea in this sample. Dramatic variations in the distribution of microorganisms within chimneys have been documented from the outer part to the inner part of the chimney, with bacteria more abundant in the cooler, more oxygen-rich outer layer of the chimney, whereas hyperthermophilic Archaea were predominant near the hot interior (15, 16). Our data are in accordance with these previous observations, because 4143-1 was from the outer layer of a venting chimney. Clone libraries were constructed for both archaeal and bacterial 16S rRNA genes. A total of 84 and 55 clones were randomly selected from the bacterial and archaeal 16S rRNA gene library for restriction fragment length polymorphism (RFLP) analyses, respectively. Representative clones of each RFLP type were sequenced. Rarefaction analysis of the bacterial and archaeal 16S rRNA gene clones suggested a much higher diversity of bacteria than archaea, as shown by the curve slopes (Fig. S2*D*).

The diverse bacterial community in 4143-1 was composed of γ-, ε-, α-, and δ-Proteobacteria, Nitrospirae, Bacteroidetes, and Planctomycetes (Fig. S2 *A* and *B*). The γ-Proteobacteria dominated the bacterial community [≈54%, represented by 6 operational taxonomic units (OTUs)], with the majority of OTUs clustering with the symbiont sequences from *Codakia orbicularis*, *Solemya terraeregina* gill, and *Ifremeria nautilei* gill (Fig. S2*B*). The symbiont γ-Proteobacteria are known to be involved in sulfur oxidation, which provides energy for their host organisms (17). The ε-Proteobacteria were the second most abundant phylotype (≈23% represented by 5 OTUs). Some of the ε-Proteobacteria are also known to be involved in sulfur oxidation (18). A large proportion of the retrieved bacterial sequences had high similarity with symbiotic bacterial sequences, implying exchange between free-living and symbiotic bacteria of similar species. These results indicated that sulfur-oxidizing bacteria could dominate the bacterial community in 4143-1.

The archaeal community in 4143-1 was relatively simple and contained exclusively Euryarchaea (Fig. S2*C*). Unidentified Euryarchaea cluster (UEII; Fig. S2*C*, cluster I) and *Thermococcus* were predominant in the library (51% and 42%, respectively). The physiology and metabolic properties for most of the archaea in 4143-1 could not be determined, because they are distinct from the known species.

Table 1. The proportion of unique genes (in bold) in each sample and a matrix representation of the overlapping number of genes between samples

	Proto-O	Proto-I	4143-1
Proto-O, Main Endeavour	**24 (4.8%)**	*6 (1.2%, 5.3%)*	*480 (95.2%, 8.8%)*
Proto-I, Main Endeavour		**51 (45.13%)**	*62 (54.9%, 1.1%)*
4143-1, Mothra			**4,878 (90.1%)**
Total no. of genes detected	504	113	5,414
Shannon Weaver's H′	5.93	5.18	6.16
Shannon Weaver's evenness	0.88	0.90	0.84
Simpson's (1/D)	45.1	28.7	48.5

When 2 different samples are compared, the italicized value indicates the number of overlapping genes between the 2 samples, and the 2 percentage values in parentheses indicate proportions of these genes in each individual sample (sample in row, sample in column).

Overview of Functional Gene Diversity. Because of the low quantity of DNA in the protochimney, whole-community genome amplification (19) was carefully performed to obtain enough DNA for microarray hybridization. On the GeoChip, there were a total of 8,371 genes from bacteria and 594 genes from archaea. After hybridization, there were 113 genes detected in Proto-I and 504 genes in Proto-O, whereas 5,414 functional genes were detected in 4143-1 (Table 1). In addition, the microbial diversity was found to be lowest in Proto-I, highest in 4143-1, and intermediate in Proto-O (Table 1). Proto-O and Proto-I had very different community compositions, as shown by the circa 1% overlapping genes between them. On the other hand, most of the genes detected in Proto-O (95%) could be found in 4143-1, suggesting that part of the microbial populations might have become stable as the chimney continued to grow. The low percentages of overlapping genes between Proto-I and Proto-O or 4143-1 indicated that a significantly different microbial community might have developed inside the cap. The fact that most of the genes detected in Proto-O were found in 4143-1 implies that common microbial populations existed in the 2 geographically different hydrothermal fields (the Main Endeavour Field vs. the Mothra Field).

Although the GeoChip contains probes from both Bacteria and Archaea, the total signal intensity of the detected probes could not be used directly to estimate the relative abundance of each in these samples, because 16 times more probes on the GeoChip are derived from Bacteria than Archaea. However, because the same arrays are used for all 3 samples under the same hybridization conditions, the relative proportions of the detected probes vs. the total probes on the arrays for both Bacteria and Archaea will stay roughly constant across these 3 samples if the ratios of Archaea to Bacteria are very similar across 3 samples and if the archaeal and bacterial probes on the arrays have similar power in detecting indigenous archaeal and bacterial populations in these samples. Thus, to further explore this idea of whether Bacteria are dominant in the matured chimney, the relative proportions of the detected archaeal or bacterial probe numbers vs. the total archaeal or bacterial probe numbers on the arrays were estimated (Fig. S3*A*). The relative proportions of the detected bacterial genes were substantially higher than those of the detected archaeal genes in 4143-1 and Proto-O, whereas they were very similar in Proto-I. These results suggested that the ratios of Archaea to Bacteria could be quite different among these 3 samples. Because the relative proportion of the detected bacterial genes was twice that of the detected archaeal genes in 4143-1, Bacteria could be dominant over Archaea in this sample, which is

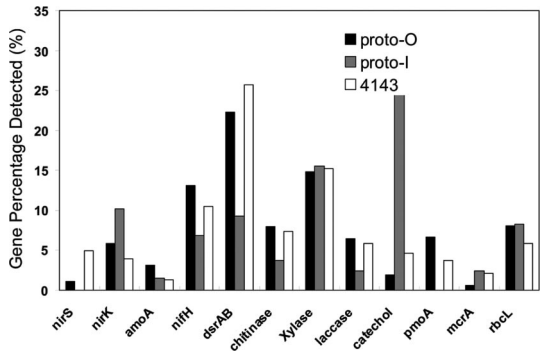

Fig. 1. Proportion of functional gene categories detected. The percentages were calculated by dividing the total signal intensity values of each gene group by total signal intensity values of all genes detected on the array.

consistent with the 16S rRNA-based quantitative PCR results described above. It should be noted that if the archaeal and bacterial probes on the arrays do not have similar power in detecting indigenous archaeal and bacterial populations in these samples, it will be difficult to use such relative proportions to infer the relative abundance of Archaea and Bacteria. Direct experimental evidence using other approaches, such as lipid biomarker analysis, are needed.

Among the genes detected, those involved in organic contaminant degradation were most abundant in all 3 samples, followed by genes involved in carbon degradation and metal resistance (Table S1). Proto-I contained significantly higher numbers of genes involved in carbon fixation and nitrification than the other 2 samples, whereas fewer genes for methane oxidation and sulfate reduction were present in Proto-I than in the other samples. The proportion of specific functional gene groups detected in the samples is presented in Fig. 1. The proportions of genes detected in Proto-O and 4143-1 showed similar variation, but were different from those detected in Proto-I. The metal-resistance genes detected are shown in Fig. S3*B* (discussed below). Because we primarily focus on carbon and nitrogen metabolisms of the chemoautotrophic communities in the chimney, genes for organic contaminant degradation and sulfate reduction will only be briefly mentioned in this paper.

Functional Community Involved in CO_2 Fixation Revealed by GeoChip. Chemolithoautotrophic microorganisms are known to be at the base of the pyramid of life because they provide food for the heterotrophic communities in the hydrothermal vents. There are, in total, 391 *rbcL* probes on the GeoChip encompassing both Form I and Form II RubisCO sequences and other RubisCO forms. Of the 391 *rbcL* probes, 10, 5, and 96 were detected in Proto-O, Proto-I, and 4143-1, respectively. The primary producers in Proto-O were similar to previously detected uncultured, deep-sea autotrophic bacteria, uncultured bacteria from groundwater, α-Proteobacterium *Rhodobacter* and *Rhodospirillum*, and *Thioalkalispira microaerophila* (Fig. S4*A*). The most dominant genes in Form I RubisCO observed here were similar to the clones from a hydrothermal vent chimney sample from TAG mound, Mid-Atlantic (20). These genes were green-like type IA, occupying about 38% of the chemosynthetic community. The most abundant genes in Form II RubisCO were similar to the clones from reducing sediment of cold seeps, symbiont bacteria of a tubeworm, and from groundwater samples (Fig. 2*A*, Fig. S4*A*, and Table S2).

In Proto-I, 5 *rbcL* genes were detected, among which 2 were from Cyanobacteria, 2 from uncultured Proteobacteria, and 1 from green sulfur bacteria. Based on signal intensity of the detected genes, *rbcL* genes from Cyanobacteria occupied 44% and green sulfur bacteria 34%, with the remaining being represented by the uncultured Proteobacteria (Fig. S4*A* and Table S2). The detection of *cbbL* genes closely related to phototrophic bacteria, including Cyanobacteria, has been documented for the dark deep-sea environment (20, 21). The similarity between the deep-sea chemoautotrophic OTUs and RubisCO from photosynthetic organisms may indicate the possible lateral transfer of RubisCO genes among deep-sea and surface water organisms (20). It should be noted that detection of *rbcL* genes in an organism does not necessarily mean that they are involved in the Calvin cycle. There are some reports demonstrating the presence of type III RubisCOs in some Archaea, but they lack the other genes in the Calvin cycle, and thus do not have the functional CBB pathway. Recently, it was found that the type III RubisCO in the archaeon *Thermococcus kodakaraensis* participates in adenosine 5-monophosphate (AMP) metabolism, distinct from the role of the classical RubisCOs in the CBB cycle (22). Previously, an obligate photosynthetic bacterial anaerobe, GSB1, was isolated from a deep-sea hydrothermal vent (23). GSB1 belongs to the green sulfur bacteria, and is related to *Chlorobium* and *Prosthecochloris* genera. The isolation of GSB1 from the vent implies that geothermal radiation and associated reduced S compounds could be sufficient to at least enhance the survival of GSB1 in the otherwise dark, oxygenated ocean depths. Here, the finding of abundant RubisCO genes of photosynthetic organisms likely supports the argument that unique photosynthetic organisms capable of harvesting geothermal radiation for growth may exist in the extremely light-deficient deep-sea hydrothermal vents; however, more direct experimental evidence is needed.

In 4143-1, Form I and Form II RubisCO genes coexisted and had comparable hybridization intensities (Fig. 2). This was verified by quantitative PCR analysis, which showed that the *cbbL* and *cbbM* gene copies were both about 10^5 copies per gram of the sample material. The main *cbbL* genes detected in 4143-1 by GeoChip belong to forms IA and IC groups (Fig. 2). Around 42% of the primary producers in the 4143-1 sample were related to deep-sea microorganisms detected previously (Fig. S4*A* and Table S2) (20).

Functional gene libraries were constructed for *cbbL* and *cbbM* to verify the GeoChip data. About 50 positive clones were randomly picked from each of the *cbbL* and *cbbM* libraries for RFLP analysis, respectively. After sequencing, 10 OTUs were obtained for *cbbL* and 7 for *cbbM* at a 3% cutoff. For *cbbL*, the clones grouped into 2 clusters (cluster I and cluster II; Fig. S4*B*), which belonged to the Form IA subfamily. No clones belonging to Form IB or Form IC were retrieved. Six OTUs in cluster I formed a distinct subgroup, which was closely related to the clones from the α- and γ-Proteobacteria. For the *cbbM* clones retrieved from 4143-1, the majority of the OTUs had the highest identity (85%) to *Magnetospirillum gryphiswaldense* MSR-1. The phylogenetic relationship of the cloned *cbbM* genes from 4143-1 with reference sequences is shown in Fig. S4*B*.

The *cbbL* and *cbbM* genes retrieved from 4143-1 by PCR amplification showed much lower diversity than those revealed by the GeoChip. Only dominant groups of sequences could be obtained by using the library construction method in our study. This may be due to the bias of the PCR primers, which preferentially target dominant groups. On the other hand, it also suggests that GeoChip hybridization might be more effective in detecting less-abundant genes. We designed specific PCR primers for several *cbbL* and *cbbM* genes, including Form IB *cbbL*, from uncultured, deep-sea autotrophic bacterium TAGI-2, and group III *cbbM* from aquifer environmental clone RA13C2II, which were detected by GeoChip hybridization but not by the library analysis. Specific PCR bands of the desired sizes for *cbbL* and *cbbM* genes were obtained, indicating that these functional genes were indeed present in the sample.

For the rTCA cycle, GeoChip only detected 2 *aclB* genes in 4143-1, which were related to uncultured episymbiont of *Alvinella pompejana* and *Chlorobium limicola*. This result suggested that the autotrophic microorganisms could predominantly use the CBB

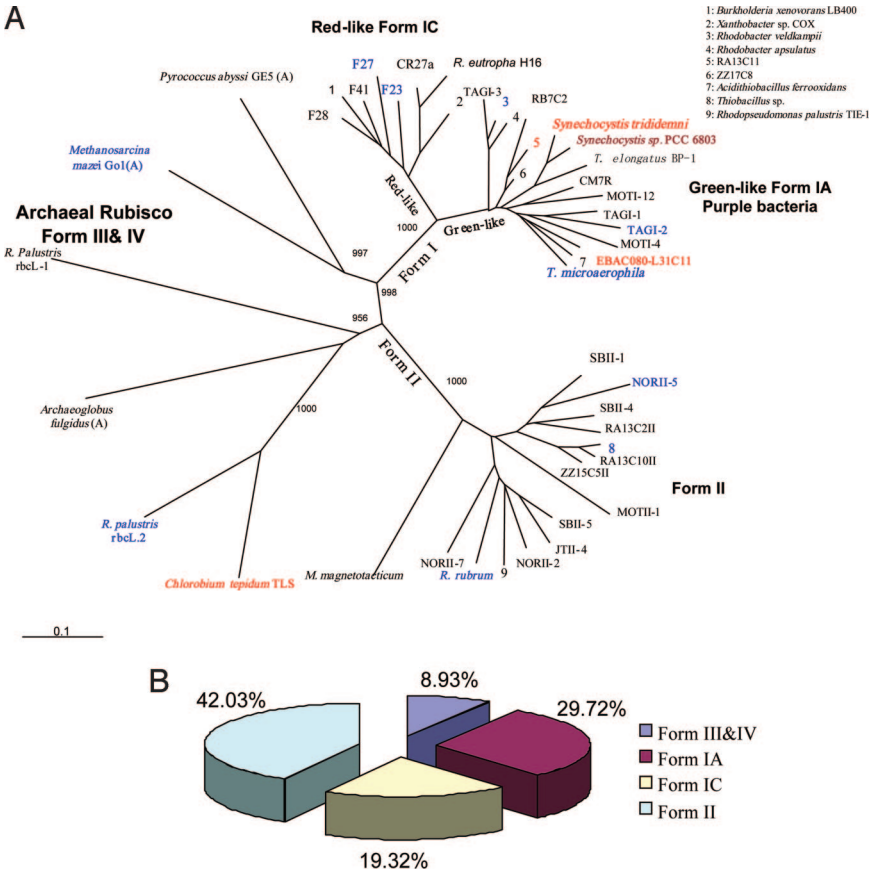

Fig. 2. Rubisco genes detected in the samples. (*A*) Phylogenetic tree based on the RubisCO large-subunit amino acid sequences obtained by GeoChip hybridization. Tree topography and evolutionary distance are given by a neighbor-joining method with Kimura distances. This tree is unrooted, with 1,000 replicates of bootstrapping. Bootstrap values are indicated only at major nodes of the tree. The designation of different colors is as follows: Red indicates unique sequences in Proto-I (4 genes), and dark red signifies the single sequence discovered in both Proto-I and 4143-1; blue designates the common sequences from both Proto-O and 4143-1 (10 genes); and black indicates the unique sequences found in 4143-1. All genes detected in Proto-I and Proto-O are listed here, but only the genes with signal intensities greater than 1 from 4143-1 were included in the tree. All genes found in Proto-O could be found in 4143-1. (Scale bar: 0.1 substitutions per site.) (*B*) Percentage of different types of *rbcL* genes detected in 4143-1.

cycle in this environment. This is, to some extent, in agreement with our species diversity analysis demonstrating that γ-Proteobacteria using the CBB cycle dominated in 4143-1, which corroborated the observation of abundant *cbbL* genes from the microarray. On the other hand, the rare detection of *aclB* genes by GeoChip may suggest that the ε-Proteobacteria in this environment contain novel *aclB* genes for the rTCA cycle. This is supported by PCR amplification using *aclB* degenerate primers, which yielded a PCR band but not the expected *aclB* genes after sequencing. We have constructed a fosmid library for 4143-1, which will allow us to determine whether this sample contains novel *aclB* genes through library screening and sequencing.

Functional Community for Methane Cycling Revealed by GeoChip. A characteristic of the thermal fluid from the Endeavour segment of the Juan de Fuca Ridge is its anomalously high CH_4 concentration (24). The CH_4 carbon isotopic compositions ($^{13}CH_4 = \approx -55‰$ vs. Pee-Dee Belemnite) of these fluids are the lightest yet found in a submarine system devoid of sediment (24). These data, in concert with the elevated CH_4 concentrations, which are up to >900 times background seawater values, likely imply a robust subseafloor methanogen community within the Endeavour system (24). The communities in the 3 chimneys were analyzed by using functional genes targeting the methane cycle. The *mcrA* gene was used to detect both methanogenesis and anaerobic methane oxidation, whereas *pmoA* was used to track aerobic methane oxidation.

Diversity of mcrA genes. Proto-O contained 2 *mcrA* genes, with one similar to *Methanothermobacter thermoautotrophicus* and the other to an uncultured euryarchaeote soil clone MCR-U3SP-12 from the Florida Everglades. Proto-I contained only 1 *mcrA* gene, which is closely related to the clone OS82 isolated from a landfill (Fig. S5 *A* and *C*).

Sample 4143-1, however, contained many more *mcrA* genes (Fig. S5 *A* and *C*). The dominant *mcrA* genes could be divided into 4 clusters belonging to Methanomicrobiales, Methanosarcinales, Methanobacteriales, and the anaerobic methane-oxidation ANME group (Fig. S5*A*). The *mcrA* gene clones in 4143-1 revealed a high diversity of methanogens and putative anaerobic methane oxidizers. The detection of clones belonging to the ANME1 and ANME2 groups implies that anoxic methane oxidation might occur in this hydrothermal vent chimney environment.

A clone library of *mcrA* was constructed for 4143-1. Phylogenetic analysis revealed that the PCR-derived *mcrA* clones of 4143-1 fall into Methanomicrobiales and Methanosarcinales (Fig. S5*A*). No ANME-related groups were detected by the PCR library analysis. Comparison of the *mcrA* genes detected on the GeoChip and *mcrA* clones from the PCR library further suggested that GeoChip could be a more sensitive gene detection method.

Diversity of pmoA sequences. Aerobic methanotrophs are a unique group of methylotrophic bacteria that use methane as their sole carbon and energy source. Based on cell morphology, ultrastructure, phylogeny, and metabolic pathways, methanotrophs can be divided into 2 taxonomic groups, type I and type II. Type I methanotrophs belong to the γ-Proteobacteria, whereas type II methanotrophs are in the α-Proteobacteria.

Several *pmoA* sequences were found in Proto-O, but none were detected in Proto-I (Fig. S5 *B* and *D*). The absence of *pmoA* sequences in Proto-I indicates that no aerobic methane oxidation had taken place, which is consistent with the fact that the hydrothermal fluid has no or limited oxygen. Aerobic methane oxidation can take place after seawater mixes with the fluid, bringing oxygen into the environment. Most of the *pmoA* sequences from Proto-O fell into the type I thermophilic methanotrophs (cluster A) and cluster B (Fig. S5*B*).

The main methanotrophic bacteria in 4143-1 contained both type I and II methanotrophs (Fig. S5 *B* and *D*). Based on GeoChip signal

intensities, type I methanotrophs were predominant and accounted for about 54% of all *pmoA* probes on the array. Type II methanotrophs accounted for about 22%, whereas the remaining 24% were from unknown species. Among the type I methanotrophs, 3 clusters (A, B, and C) could be observed, with cluster A sequences predominating (64%). Cluster A consisted of sequences from a thermophilic methanotroph strain HB and *pmoA* clones from deep-sea hydrothermal vents (11). Cluster B contained clones from organic soil and Lake Washington sediment. Cluster C contained clones from a Movile cave (Fig. S5*B*).

Functional Community for Nitrogen Cycle Revealed by GeoChip. ***Diversity of nifH sequences.*** Dissolved dinitrogen gas (N_2) is abundant in deep seawater and in hot hydrothermal vent fluids. Nitrogen isotope ratios ($^{15}N/^{14}N$) of vent animals are much lower than the ratios of deep-sea organic nitrogen, ammonium, and nitrate, but are similar to those of deep oceanic N_2 and marine biota associated with nitrogen fixation (25). Recently, a thermophilic methanogen capable of nitrogen fixation at 92 °C was isolated from the hydrothermal vent environment (26). All data indicate that biological nitrogen fixation is an important process of nitrogen cycling in the vent environments. Biological nitrogen fixation uses the nitrogenase enzyme complex encoded by *nifHDK* to reduce dissolved N_2 to ammonium (NH_4^+). *nifH* encodes the iron-containing protein and is highly conserved among various microorganisms. All *nifH* genes fall into 4 clusters: cluster I includes standard molybdenum nitrogenases from Cyanobacteria and Proteobacteria (α, β, γ), as well as *nvfH* from γ-Proteobacteria; cluster II includes methanogen nitrogenases and bacterial *anfH*; cluster III is composed of nitrogenases from diverse anaerobic bacteria, such as Clostridia and δ-Proteobacterial sulfate reducers; cluster IV includes nitrogenases from methanogens (10).

In this study, results from GeoChip showed an increasing number of *nifH* genes across samples: 5 in Proto-I, 20 in Proto-O, and 58 in 4143-1. Cluster III *nifH* genes were dominant in all samples (Fig. S6). Among the 5 *nifH* genes detected from Proto-I, 4 of them fell in *nifH* cluster III, and one in cluster IV. This is a good reflection of the strict anaerobic environment of Proto-I. The *nifH* genes in Proto-O fell into clusters I, III, and IV, with cluster III being predominant (around 70%). The main *nifH* genes in Proto-O were from unidentified or uncultured bacteria retrieved from different environments.

Sample 4143-1, again, contained significantly more *nifH* genes than Proto-O and Proto-I, and they were distributed among all 4 clusters. Cluster III *nifH* genes were dominant (59.9%), followed by cluster I sequences (27.6%). The archaeal *nifH* genes distributed in clusters II and IV only constituted a small proportion of the total *nifH* genes. This is consistent with the quantification results of microbial 16S rRNA genes, which showed that bacteria were predominant in the sample.

Genes involved in nitrification and denitrification. Nitrification and denitrification have been observed in the hydrothermal environments (27, 28). The GeoChip contains extensive probes targeting genes involved in nitrification, such as *amo* (ammonia monooxygenase), and nitrogen metabolism, such as *gdh* (glutamate dehydragenase), *nasA* (assimilatory nitrate reductase), *nar* (nitrate reductase), *nir* (nitrite reductase), *norB* (nitric oxide reductase), and *nosZ* (nitrous oxide reductase). Most of these essential genes involved in nitrification and denitrification were detected in all 3 samples. However, the genes detected from Proto-I and Proto-O were completely different, indicating different microorganisms might be involved in these processes. In 4143-1, the majority of the *amoA* sequences were from *Nitrosomonas* and uncultivated β-Proteobacteria. Crenarchaeotal *amoA* genes were also detected (Fig. S7*A*). The presence of archaeal *amoA* genes was confirmed by positive PCR amplification using archaeal *amoA*-specific primers; however, PCR amplification of bacterial *amoA* genes failed. The nitrifying archaea may be derived from mixing of seawater with the vent fluid or from thermophilic nitrifying archaea in the chimney, because thermophilic and moderately thermophilic nitrifying archaea have been enriched from hot spring environments (29–31). Most of the *nir* sequences detected were from uncultured organisms from various environments (Fig. S7 *B* and *C*). Our results provide the genetic evidence for possible existence of nitrification and denitrification in deep-sea hydrothermal vent chimneys. This is consistent with the observation of the relatively high ammonia concentrations in some chimney environments in Juan de Fuca Ridge (24), suggesting that nitrification could be an important process in deep-sea hydrothermal vents.

Genes for Metal Resistance Revealed by GeoChip. The deep-sea hydrothermal vent environment is rich in various heavy metals. Microorganisms are known to respond or adapt to potentially toxic levels of iron through multiple strategies, including dissimilatory and assimilatory metal oxidation and reduction, as well as metal transport (32). Much more is known regarding dissimilatory reactions than assimilatory reactions, although most studies have focused on mesophilic microbes. Many microorganisms isolated from hydrothermal environments are metal-resistant. Generally, metal-resistance mechanisms of microorganisms from hydrothermal vents are similar to those of mesophilic organisms isolated from other environments; however, novel mechanisms for metal reduction in hyperthermophilic archaea have been observed (33). It would be difficult to detect novel metal-resistance mechanisms by using GeoChip, because only known sequences are covered by the array. However, this study allows a careful survey and comparison of genes putatively involved in metal resistance from hydrothermal vent environments at the community level.

In Proto-I, most of the detected metal resistance genes were for cadmium, tellurium, aluminum, and chromium resistance (Fig. S3*B*). In Proto-O and 4143-1, the majority of resistance genes were for arsenic and mercury, with the remaining being for chromium, tellurium, and other metals (Fig. S3*B*). The data imply that microorganisms in Proto-I may be generally resistant to chromium and tellurium but more sensitive to arsenic and mercury.

Other Main Genes Revealed by GeoChip. Large numbers of genes detected by the GeoChip also included those involved in sulfate reduction and carbon/organic contaminant degradation. Sulfate reduction is thought to be one of the important energy sources for microbial systems at hydrothermal vents (34). Only 3 *dsrB* genes were detected in Proto-I, which are related to those found in *Desulfotomaculum geothermicum*, a thermophilic Firmicutes originally isolated from geothermal ground water; *Syntrophobacter fumaroxidans*, an H_2-producing syntroph of δ-Proteobacteria; and an unidentified clone from groundwater at a uranium mill tailings site. The *dsr* genes detected in Proto-O and 4143-1 were highly diverse and were related to those in Desulfobacteraceae, Desulfovibrionaceae, Peptococcaceae, Desulfobulbacaea, Syntrophobacteraceae, and unidentified clusters.

Little is known about carbon and organic contaminant degradation and their contribution to the vent ecosystems. GeoChip analysis revealed that carbon degradation genes are highly abundant in these vent systems, suggesting that they may play important roles in carbon cycling and metabolism in the geothermal environment. However, further studies are needed in terms of carbon cycling processes and their associated microbial communities. It should be noted that many genes classified in the category of organic contaminant degradation (e.g., aromatic degradation genes) are also important in the degradation of various carbon polymers in nature. Thus, the detection of these types of genes does not necessarily indicate the existence of such contaminants in the vent systems.

Summary. In this study, GeoChip hybridization, clone libraries, and quantitative PCR were integrated to examine the abundance and

metabolic diversity of microbial populations in the Juan de Fuca hydrothermal vent chimneys. Microbial populations detected by the GeoChip were significantly higher than estimates based on gene clone library analyses but were consistent with the observation of a vast diversity of microorganisms in the hydrothermal vents revealed by extensive (hundreds of thousands of sequences) sequencing analysis (35). Significant variability of functional genes related to carbon, sulfur, and nitrogen metabolism was observed during the development of vent chimneys. This may be due to the changing vent structure and chemical composition. By 16S rRNA gene library analysis, bacteria affiliated within γ- and ε-Proteobacteria groups were dominant in 4143-1. Quantitative PCR analysis of 16S rRNA genes suggested that Bacteria could be more abundant than Archaea in 4143-1. The primary producers in the 3 samples could primarily use the CBB cycle. In particular, photosynthetic green-like *cbbL* genes were the major components in Proto-I, whereas previously retrieved *cbbL* and *cbbM* genes from deep-sea hydrothermal vents were predominant in Proto-O and 4143-1. Clone libraries using the 16S rRNA and functional genes (*mcrA*, *cbbL*, *cbbM*) supported the GeoChip results but were less effective than the microarray technology in delineating the microbial community structure of low-biomass communities. Our study revealed extremely rich and diverse metabolic reservoirs of the microbial community in the hydrothermal vent chimney environment, which has not been fully recognized before. Furthermore, our data showed the great potential of high-throughput microarray technology in understanding ecosystem dynamics in the complex hydrothermal vent environments.

Materials and Methods

Samples from the sulfide chimneys were collected by the submersible Alvin supported by the R/V Atlantis in 2005 and 2006 at the Endeavour Segment of the Juan de Fuca Ridge, located ≈300 km west of Vancouver Island, Canada. During a cruise in 2006, a stainless steel cap was deployed on top of a chimney that was vigorously venting at the Maine Endeavour field (Fig. S1). The fluid temperature was higher than 300 °C. After 15 days of deployment, samples were collected from the chimney formed on top of the cap (Proto-O; Fig. S1) and the sulfate deposit accumulated on the surface of the inner cap (Proto-I). An outer part of a mature sulfide chimney (4143-1) collected in 2005 from the Mothra Field, which was venting at about 316 °C at the time of sampling, was also used for comparison. Precautions were taken during sampling and handling of the chimney samples to preserve their integrity for microbiological analyses. The chimneys were stored at −20 °C as soon as collected, kept on dry ice during transportation, and stored at −80 °C until further analysis.

The methods of molecular manipulations, including DNA isolation, amplification, labeling, and microarray hybridization; construction of 16S rRNA, *mcrA*, *cbbL*, and *cbbM* gene clone libraries; and quantitative PCR are essentially based on established methods described previously (19, 20, 36–40). Sequences obtained for bacterial and archaeal 16S rRNA, *mcrA*, *cbbL*, and *cbbM* genes were deposited in the GenBank database under accession numbers FJ640793–FJ640842. The details are provided as *SI Methods*.

ACKNOWLEDGMENTS. We thank Maurice A. Tivey (Woods Hole Oceanographic Institution, Woods Hole, MA), Marvin D. Lilley (University of Washington, Seattle, WA), Deborah Kelly (University of Washington, Seattle, WA), Kang Ding (University of Minnesota, Minneapolis, MN), and all of the crew members from R/V Atlantis/DSV Alvin for their efforts and help in sample collection. This study was supported by China Ocean Mineral Resources R&D Association Grant DYXM-115-02-2-01), by National Natural Science Foundation of China Grants 40532011, 40403004, and 40473032, and by the U.S. Department of Energy under the Genomics: GTL program through the Virtual Institute of Microbial Stress and Survival (http://vimss.lbl.gov), Office of Biological and Environmental Research, Office of Science.

1. Francheteau J, et al. (1979) Massive deep-sea sulfide ore deposits discovered on the East Pacific Rise. *Nature* 277:523–528.
2. Zierenberg RA, Adams MW, Arp AJ (2000) Life in extreme environments: Hydrothermal vents. *Proc Natl Acad Sci USA* 97:12961–12962.
3. Deming JW, Baross JA (1993) Deep-sea smokers: Windows to a subsurface biosphere? *Geochim Cosmochim Acta* 57:3219–3230.
4. Kelley DS, Baross JA, Delaney JR (2002) Volcanoes, fluids, and life at mid-ocean ridge spreading centers. *Annu Rev Earth Planet Sci* 30:385–491.
5. Kristall B, Kelly DS, Hannington MD, Delaney JR (July 4, 2006) Growth history of a diffusely venting sulfide structure from the Juan de Fuca ridge: A petrological and geochemical study. *Geochem Geophys Geosyst*, 10.1029/2005GC001166.
6. Huber JA, Butterfield DA, Baross JA (2002) Temporal changes in archaeal diversity and chemistry in a mid-ocean ridge subseafloor habitat. *Appl Environ Microbiol* 68:1585–1594.
7. Nercessian O, Reysenbach AL, Prieur D, Jeanthon C (2003) Archaeal diversity associated with in situ samplers deployed on hydrothermal vents on the East Pacific Rise (13 degrees N). *Environ Microbiol* 5:492–502.
8. McCliment EA, et al. (2006) Colonization of nascent, deep-sea hydrothermal vents by a novel Archaeal and Nanoarchaeal assemblage. *Environ Microbiol* 8:114–125.
9. Page A, Tivey MK, Stakes DS, Reysenbach AL (2008) Temporal and spatial archaeal colonization of hydrothermal vent deposits. *Environ Microbiol* 10:874–884.
10. Mehta MP, Butterfield DA, Baross JA (2003) Phylogenetic diversity of nitrogenase (*nifH*) genes in deep-sea and hydrothermal vent environments of the Juan de Fuca Ridge. *Appl Environ Microbiol* 69:960–970.
11. Nercessian O, Bienvenu N, Moreira D, Prieur D, Jeanthon C (2005) Diversity of functional genes of methanogens, methanotrophs and sulfate reducers in deep-sea hydrothermal environments. *Environ Microbiol* 7:118–132.
12. Reysenbach AL, Shock E (2002) Merging genomes with geochemistry in hydrothermal ecosystems. *Science* 296:1077–1082.
13. He Z, et al. (2007) GeoChip: A comprehensive microarray for investigating biogeochemical, ecological and environmental processes. *Isme J* 1:67–77.
14. Zhou J, Kang S, Schadt CW, Garten CTJ (2008) Spatial scaling of functional gene diversity across various microbial taxa. *Proc Natl Acad Sci USA* 105:7768–7773.
15. Harmsen H, Prieur D, Jeanthon C (1997) Distribution of microorganisms in deep-sea hydrothermal vent chimneys investigated by whole-cell hybridization and enrichment culture of thermophilic subpopulations. *Appl Environ Microbiol* 63:2876–2883.
16. Schrenk MO, Kelley DS, Delaney JR, Baross JA (2003) Incidence and diversity of microorganisms within the walls of an active deep-sea sulfide chimney. *Appl Environ Microbiol* 69:3580–3592.
17. Duperron S, Laurent MC, Gaill F, Gros O (2008) Sulphur-oxidizing extracellular bacteria in the gills of Mytilidae associated with wood falls. *FEMS Microbiol Ecol* 63:338–349.
18. Campbell BJ, Engle AS, Porter ML, Takai K (2006) The versatile epsilon-Proteobacteria: Key players in sulphidic habitats. *Nat Rev Microbiol* 4:458–468.
19. Wu L, Liu X, Schadt CW, Zhou J (2006) Microarray-based analysis of subnanogram quantities of microbial community DNAs by using whole-community genome amplification. *Appl Environ Microbiol* 72:4931–4941.
20. Elsaied H, Naganuma T (2001) Phylogenetic diversity of ribulose-1,5-bisphosphate carboxylase/oxygenase large-subunit genes from deep-sea microorganisms. *Appl Environ Microbiol* 67:1751–1765.
21. Elsaied HE, Kimura H, Naganuma T (2007) Composition of archaeal, bacterial, and eukaryal RuBisCO genotypes in three Western Pacific arc hydrothermal vent systems. *Extremophiles* 11:191–202.
22. Sato T, Atomi H, Imanaka T (2007) Archaeal type III RuBisCOs function in a pathway for AMP metabolism. *Science* 315:1003–1006.
23. Beatty JT, et al. (2005) An obligately photosynthetic bacterial anaerobe from a deep-sea hydrothermal vent. *Proc Natl Acad Sci USA* 102:9306–9310.
24. Lilley MD, et al. (1993) Anomalous CH_4 and NH_4^+ concentrations at an unsedimented mid-ocean-ridge hydrothermal system. *Nature* 364:45–47.
25. Rau GH (1981) Low $^{15}N/^{14}N$ in hydrothermal vent animals: Ecological implications. *Nature* 289:484–485.
26. Mehta MP, Baross JA (2006) Nitrogen fixation at 92 degrees C by a hydrothermal vent archaeon. *Science* 314:1783–1786.
27. Jannasch HW (1984) In *Hydrothermal Processes at Seafloor Spreading Centers*, eds Rona PA, Bostrom K, Laubier L, Smith KL (Plenum, New York), pp 677–709.
28. Lilley M, Baross JA, Gordon LI (1984) In *Hydrothermal Processes at Seafloor Spreading Centers*, eds Rona PA, Bostrom K, Laubier L, Smith KL (Plenum, New York), pp 411–449.
29. Hatzenpichler R, et al. (2008) A moderately thermophilic ammonia-oxidizing crenarchaeote from a hot spring. *Proc Natl Acad Sci USA* 105:2134–2139.
30. de la Torre JR, Walker CB, Ingalls AE, Konneke M, Stahl DA (2008) Cultivation of a thermophilic ammonia oxidizing archaeon synthesizing crenarchaeol. *Environ Microbiol* 10:810–818.
31. Zhang CL, et al. (2008) Global occurrence of archaeal amoA genes in terrestrial hot springs. *Appl Environ Microbiol* 74:6417–6426.
32. Holden JF, Adams MW (2003) Microbe-metal interactions in marine hydrothermal environments. *Curr Opin Chem Biol* 7:160–165.
33. Childers SE, Lovley DR (2001) Differences in Fe(III) reduction in the hyperthermophilic archaeon, Pyrobaculum islandicum, versus mesophilic Fe(III)-reducing bacteria. *FEMS Microbiol Lett* 195:253–258.
34. Nakagawa T, Nakagawa S, Inagaki F, Takai K, Horikoshi K (2004) Phylogenetic diversity of sulfate-reducing prokaryotes in active deep-sea hydrothermal vent chimney structures. *FEMS Microbiol Lett* 232:145–152.
35. Huber JA, et al. (2007) Microbial population structures in the deep marine biosphere. *Science* 318:97–100.
36. Zhou J, Bruns MA, Tiedje JM (1996) DNA recovery from soils of diverse composition. *Appl Environ Microbiol* 62:316–322.
37. Yergeau E, Kang S, He Z, Zhou J, Kowalchuk GA (2007) Functional microarray analysis of nitrogen and carbon cycling genes across an Antarctic latitudinal transect. *Isme J* 1:163–179.
38. Wu L, et al. (2004) Development and evaluation of microarray-based whole-genome hybridization for detection of microorganisms within the context of environmental applications. *Environ Sci Technol* 38:6775–6782.
39. Hales BA, et al. (1996) Isolation and identification of methanogen-specific DNA from blanket bog peat by PCR amplification and sequence analysis. *Appl Environ Microbiol* 62:668–675.
40. Campbell BJ, Stein JL, Cary SC (2003) Evidence of chemolithoautotrophy in the bacterial community associated with Alvinella pompejana, a hydrothermal vent polychaete. *Appl Environ Microbiol* 69:5070–5078.

Supporting Information

Wang et al. 10.1073/pnas.0810418106

SI Methods

DNA Isolation, Amplification, Labeling, and Microarray Hybridization. The genomic DNA was isolated from the chimneys (1) and amplified by using 50 ng of DNA as described previously (2). The amplified DNA was fluorescently labeled with cy5 dye (GE Healthcare) by using random primers and Klenow (large fragment of DNA polymerase I; Invitrogen) according to the manufacturer's directions. The microarray hybridization was conducted at 50 °C in the presence of 50% formamide, as previously described (3). All hybridization experiments were carried out in duplicate.

Microarray Scanning and Data Processing. A ScanArray 500 microarray system (PerkinElmer) was used for scanning the microarray slides. Scanned images were processed by using ImaGene, version 5.0 (Biodiscovery), as described previously (4). The signal-to noise ratio (SNR) was calculated based on the formula: SNR = (signal intensity − background)/standard deviation of background. Spots with SNR greater or equal to 3 were regarded as positive. Data processing, such as outlier removal, normalization, and poor spot removal, was carried out as previously described (2).

Constructing 16S rRNA, *mcrA*, *cbbL*, and *cbbM* Gene Clone Libraries. The archaeal and bacterial 16S rRNA gene clone libraries were constructed by using universal primer sets Arch 27F/958R and Bac21F/1492R, respectively. RubisCO Form I *cbbL* genes were amplified with primers 595F/1387R with an 800-bp fragment, whereas Form II *cbbM* genes were amplified with cbbM663F/cbbM1033R, which yields a 400-bp fragment (5). The *mcrA* gene was amplified with primers ME1 and ME2 (6). The PCR products were purified on a 1% agarose gel, extracted with a gel-extraction kit (Omega Bio-Tek Inc.). Afterward, the purified DNA products were ligated with the pMD18-T vector (Takara) and transformed to competent cells of *Escherichia coli* DH-5α according to the manufacturer's instructions.

Quantitative PCR. Serial dilutions of positive control DNA were used as calibration standards for the quantitative real-time PCR. The positive control DNA extracts were amplified with the *cbbM* primers (328 bp) (7), with sulfide-chimney DNA from this study as the template. The resulting amplicons were purified with a gel-extraction kit (Omega Bio-Tek Inc.) as recommended by the manufacturer, and were cloned to the pMD18-T vector. After reamplification with vector-specific primers according to the manufacturer's instructions, the PCR products were purified as described above. The PCR products obtained were then quantified with the NanoDrop ND-1000 spectrophotometer (NanoDrop Technologies). The measured DNA amount was converted to target molecule numbers per microliter, and the *cbbM* standards were adjusted to 10^{10} target molecules per microliter by serial dilution. PCR and monitoring of SYBR Green I fluorogenic probe signals were performed by using an ABI Prism 7500 (Applied Biosystems). Copy numbers of the *cbbL* gene were determined by quantitative competitive PCR (QC-PCR). The liner plasmid pmD-18T Δ150bp was used as the competitive template DNA. PCR products were separated by electrophoresis using 2.0% (wt/vol) agarose with TBE buffer (90 mM Tris, 90 mM boric acid, and 2 mM Na_2-EDTA; pH 8.0) and were stained with ethidium bromide. The copy number of the target gene was estimated by considering the band intensity and sizes of target and standard DNA and the initial concentration of *cbbL* present in chimney DNA; this concentration was subsequently adjusted to obtain a gene copy value on a wet-weight basis.

1. Zhou J, Bruns MA, Tiedje JM (1996) DNA recovery from soils of diverse composition. *Appl Environ Microbiol* 62:316–322.
2. Wu L, Liu X, Schadt CW, Zhou J (2006) Microarray-based analysis of subnanogram quantities of microbial community DNAs by using whole-community genome amplification. *Appl Environ Microbiol* 72:4931–4941.
3. Yergeau E, Kang S, He Z, Zhou J, Kowalchuk GA (2007) Functional microarray analysis of nitrogen and carbon cycling genes across an Antarctic latitudinal transect. *Isme J* 1:163–179.
4. Wu L, et al. (2004) Development and evaluation of microarray-based whole-genome hybridization for detection of microorganisms within the context of environmental applications. *Environ Sci Technol* 38:6775–6782
5. Elsaied H, Naganuma T (2001) Phylogenetic diversity of ribulose-1,5-bisphosphate carboxylase/oxygenase large-subunit genes from deep-sea microorganisms. *Appl Environ Microbiol* 67:1751–1765.
6. Hales BA, et al. (1996) Isolation and identification of methanogen-specific DNA from blanket bog peat by PCR amplification and sequence analysis. *Appl Environ Microbiol* 62:668–675.
7. Campbell BJ, Stein JL, Cary SC (2003) Evidence of chemolithoautotrophy in the bacterial community associated with Alvinella pompejana, a hydrothermal vent polychaete. *Appl Environ Microbiol* 69:5070–5078.

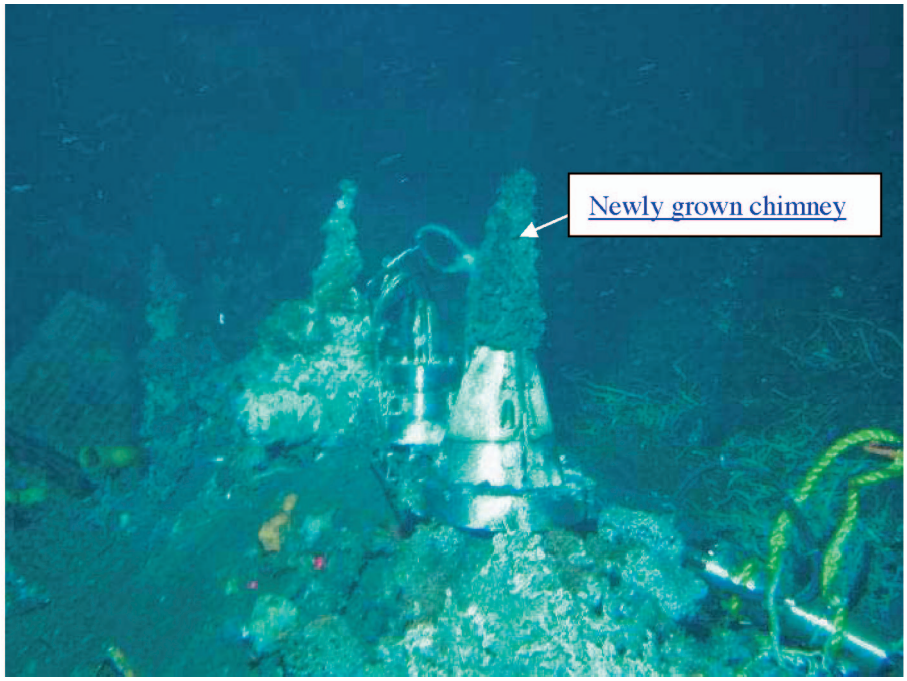

Fig. S1. A photo showing a newly grown chimney from the opening of the stainless steel cap deployed on top of a chimney venting at ≈316 °C at Main Endeavour, Juan de Fuca Ridge.

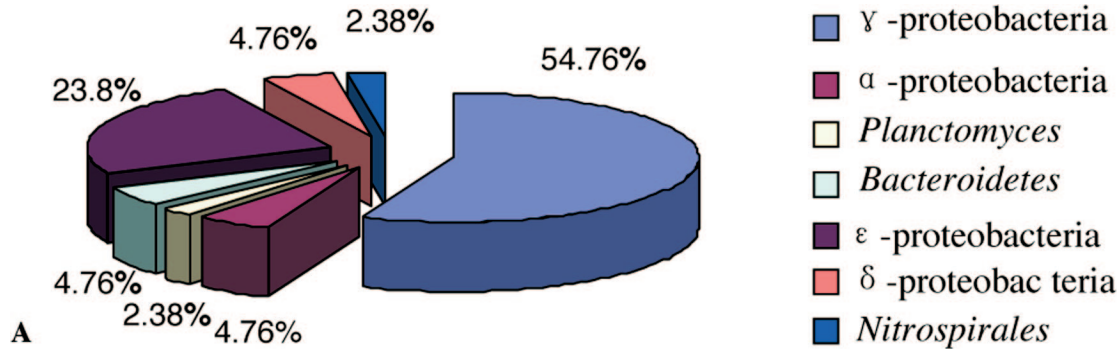

Fig. S2. Microbial community diversity of 16S rRNA gene analysis in 4143-1. (*A*) Proportion of different bacterial divisions within the bacterial community of 4143-1. The percentage was calculated by dividing the number of OTUs in the bacterial division with the total number of sequenced bacterial 16S rRNA gene clones. (B) Phylogenetic tree constructed from bacterial 16S rRNA gene sequences. The phylogenetic relationships among the retrieved bacterial 16S rRNA gene sequences from 4143-1 and the reference sequences from GenBank are shown. The tree was inferred by neighbor-joining analysis of 16S rRNA gene sequences with software Mega 4.0 (Center of Evolutionary Functional Genomics, Biodesign Institute, Arizona State University). Clones from this study are shown in bold. The numbers in parentheses are the GenBank accession numbers for sequences obtained from the National Center for Biotechnology Information database. Bootstrap percentages were obtained by using 1,000 replicates, and values greater than 50% are indicated at the nodes. The scale bar represents 5% of changes per nucleotide position. (*C*) Phylogenetic tree constructed from archaeal 16S rRNA gene sequences. (*D*) Rarefaction curves for bacterial and archaeal 16S rRNA sequences from 4143-1 sample.

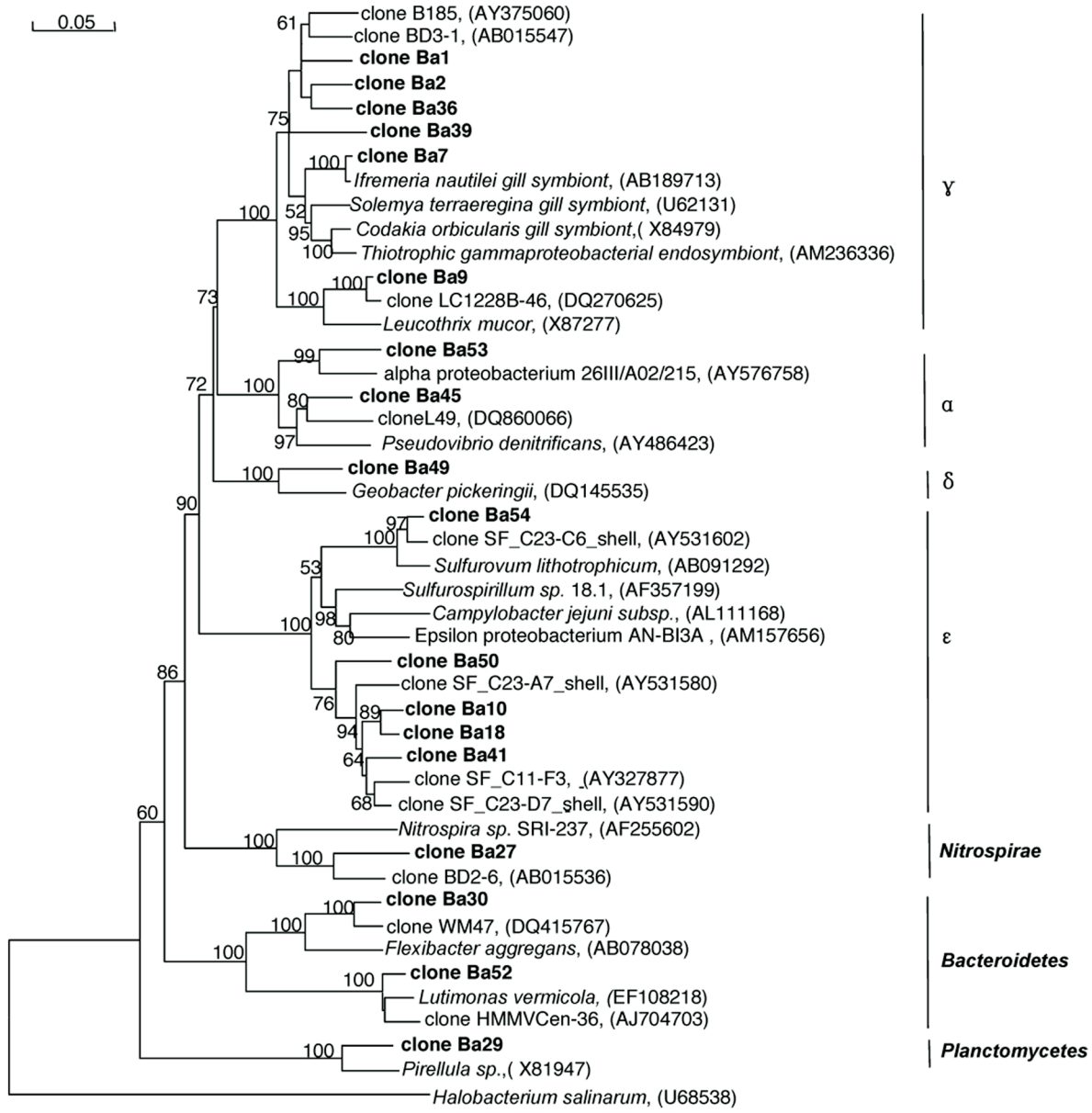

B

Fig. S2. Continued.

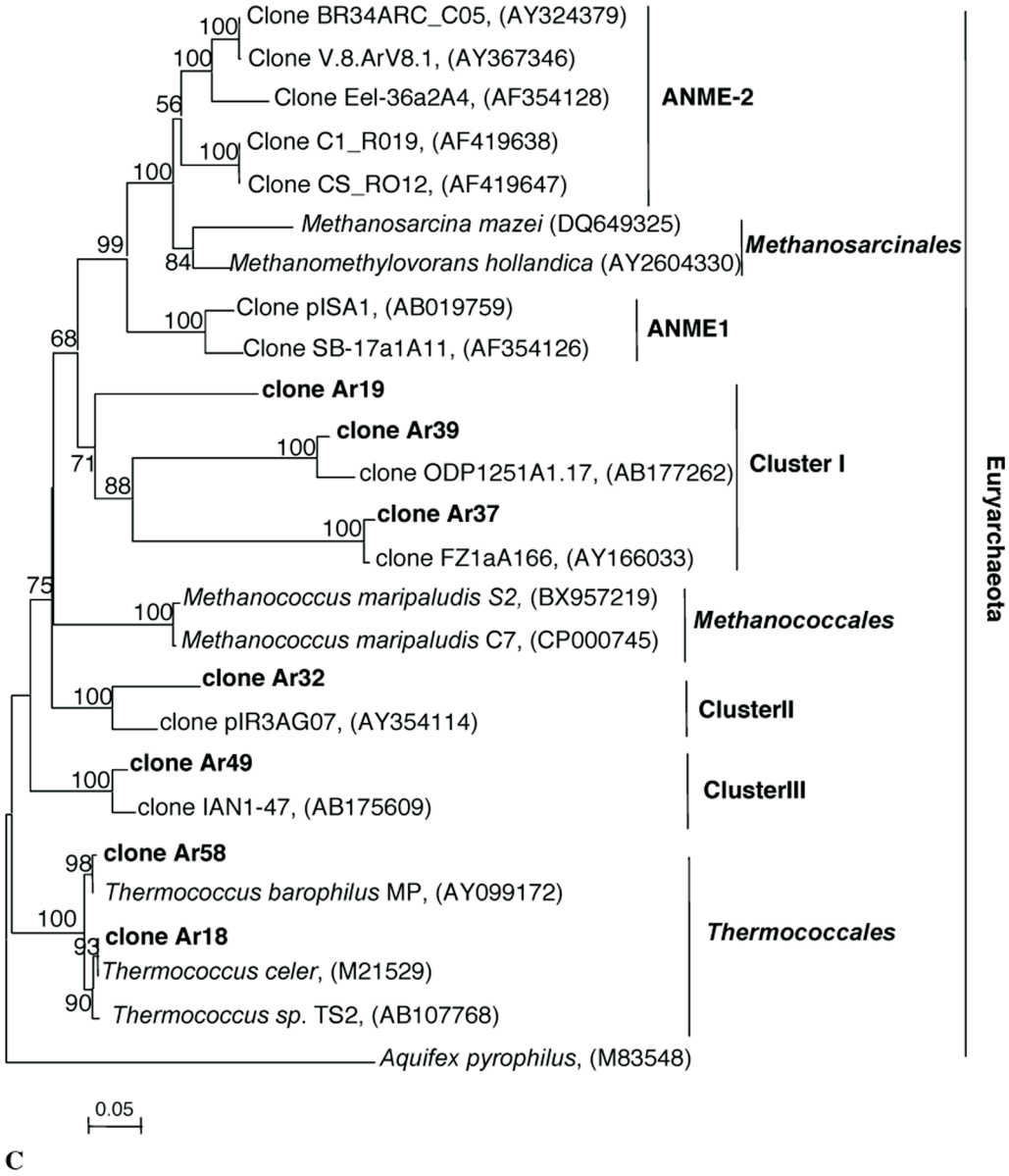

C

Fig. S2. Continued.

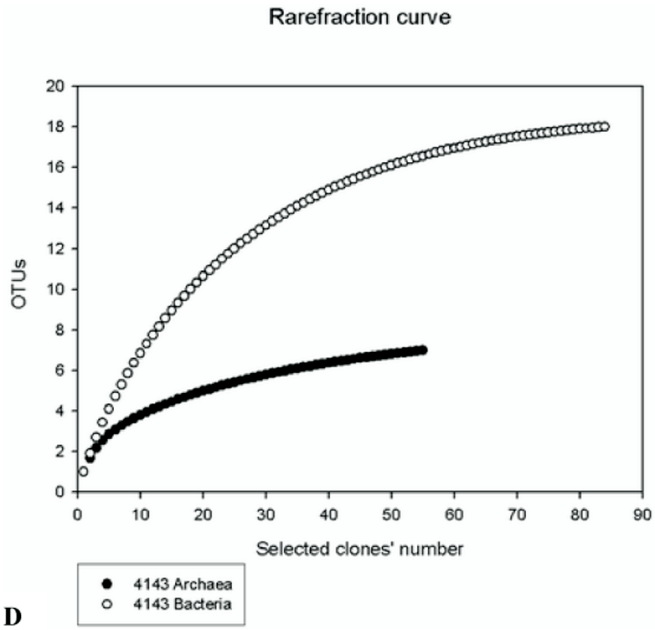

D

Fig. S2. Continued.

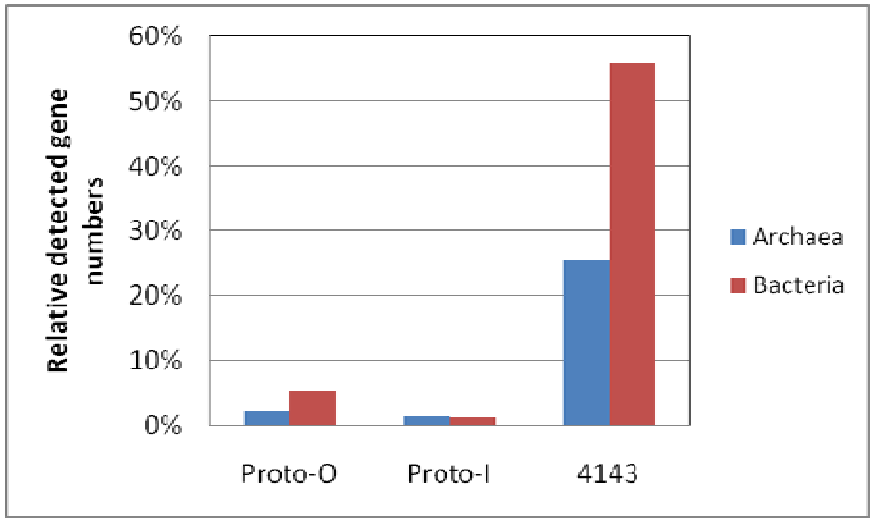

A

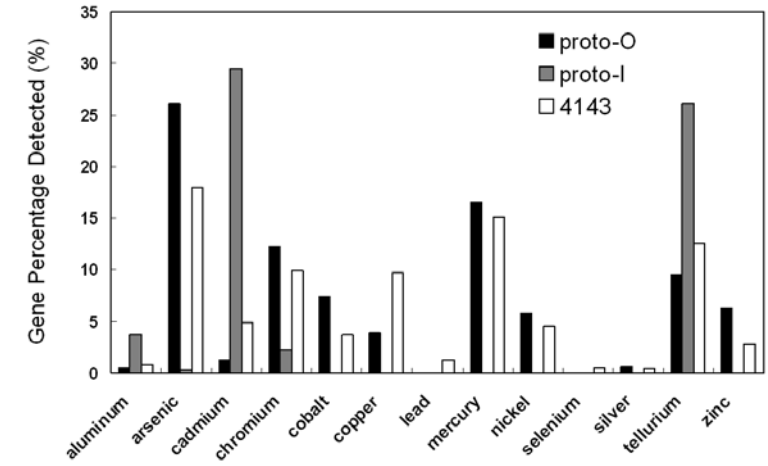

B

Fig. S3. Relative abundance of genes detected. (*A*) Relative proportions of detected archaeal or bacterial gene numbers from the chimney samples versus their respective total gene numbers on the chip. There are a total of 8,371 and 594 genes from Bacteria and Archaea on the chip, respectively. (*B*) Percentage of genes for metal resistance. The percentage of genes involved in aluminum, arsenic, cadmium, chromium, cobalt, copper, lead, mercury, nickel, selenium, silver, tellurium, and zinc were calculated by dividing the total signal intensity values for each individual metal-resistance group by the total intensity values of all metal-resistance genes detected on the array.

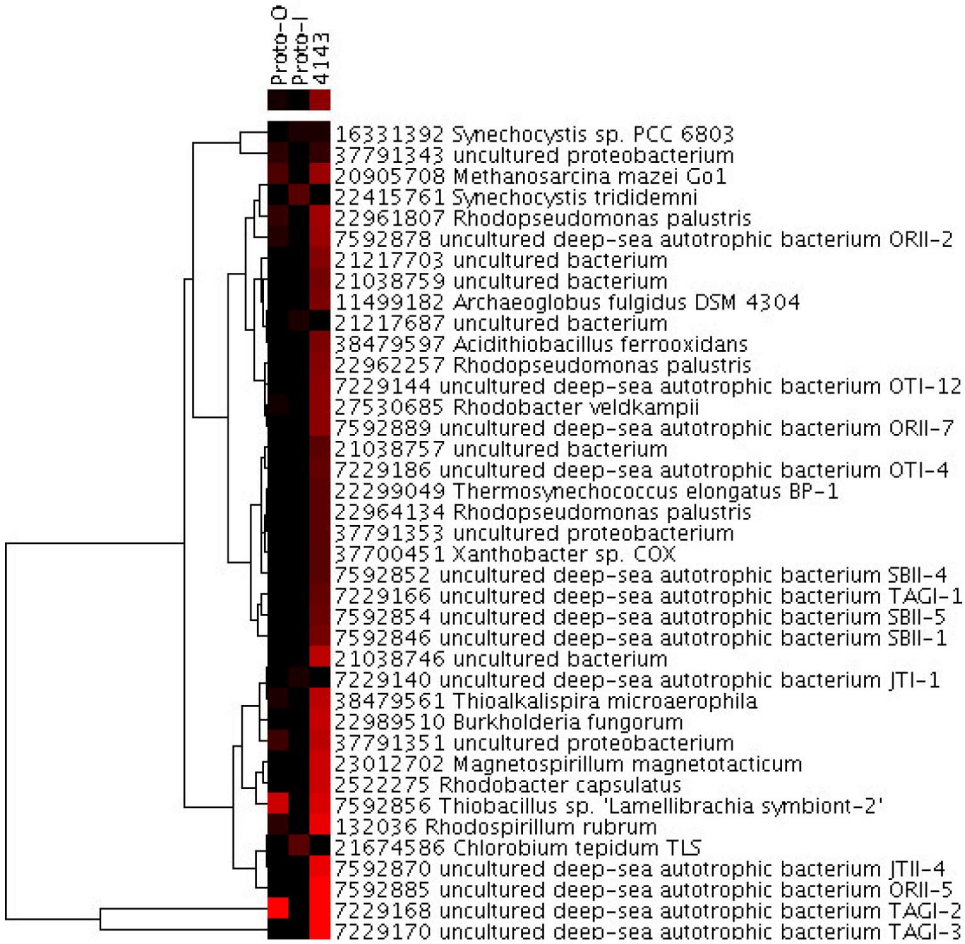

A

Fig. S4. Analysis of CO_2 fixation genes detected. (*A*) Hierarchical cluster analysis of *rbcL* genes based on hybridization signals for Proto-I, Proto-O, and 4143-1. The figure was generated by using CLUSTER (http://rana.lbl.gov/EisenSoftware.htm) and visualized with TREEVIEW (http://rana.lbl.gov/EisenSoftware.htm). Black represents no hybridization above background level, and red represents positive hybridization. The color intensity indicates differences in hybridization patterns. All genes detected in Proto-I and Proto-O are listed, but only the genes with signal intensities greater than 1 from 4143-1 were included here. (*B*) Phylogenetic tree based on the deduced amino acid sequences of RubisCO large-subunit genes. Clone sequences (OTUs) retrieved from *cbbL* and *cbbM* clone libraries are indicated in bold. (Scale bar: 0.1 substitutions per site.) See the Fig. S2*B* legend for details.

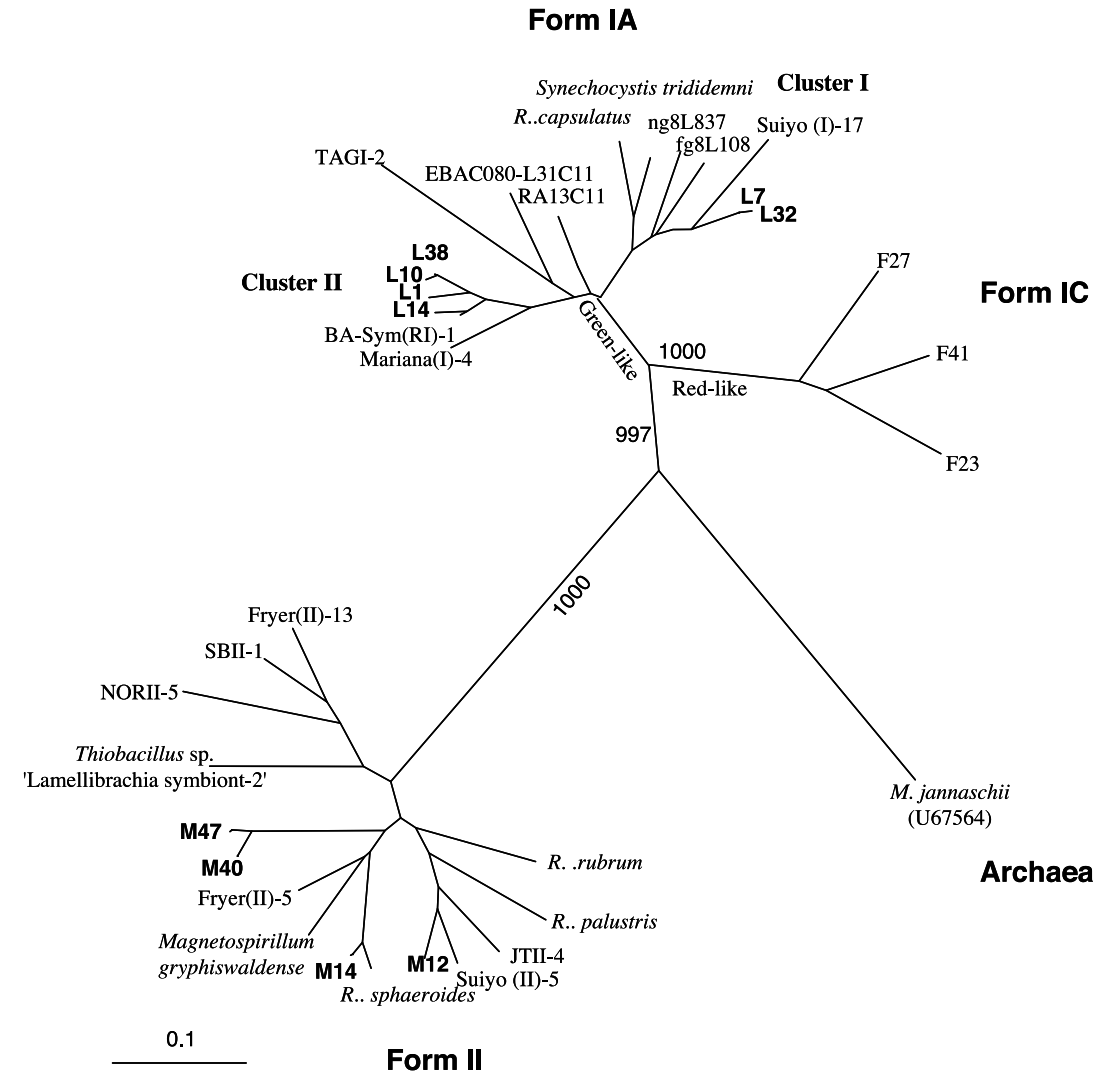

B

Fig. S4. Continued.

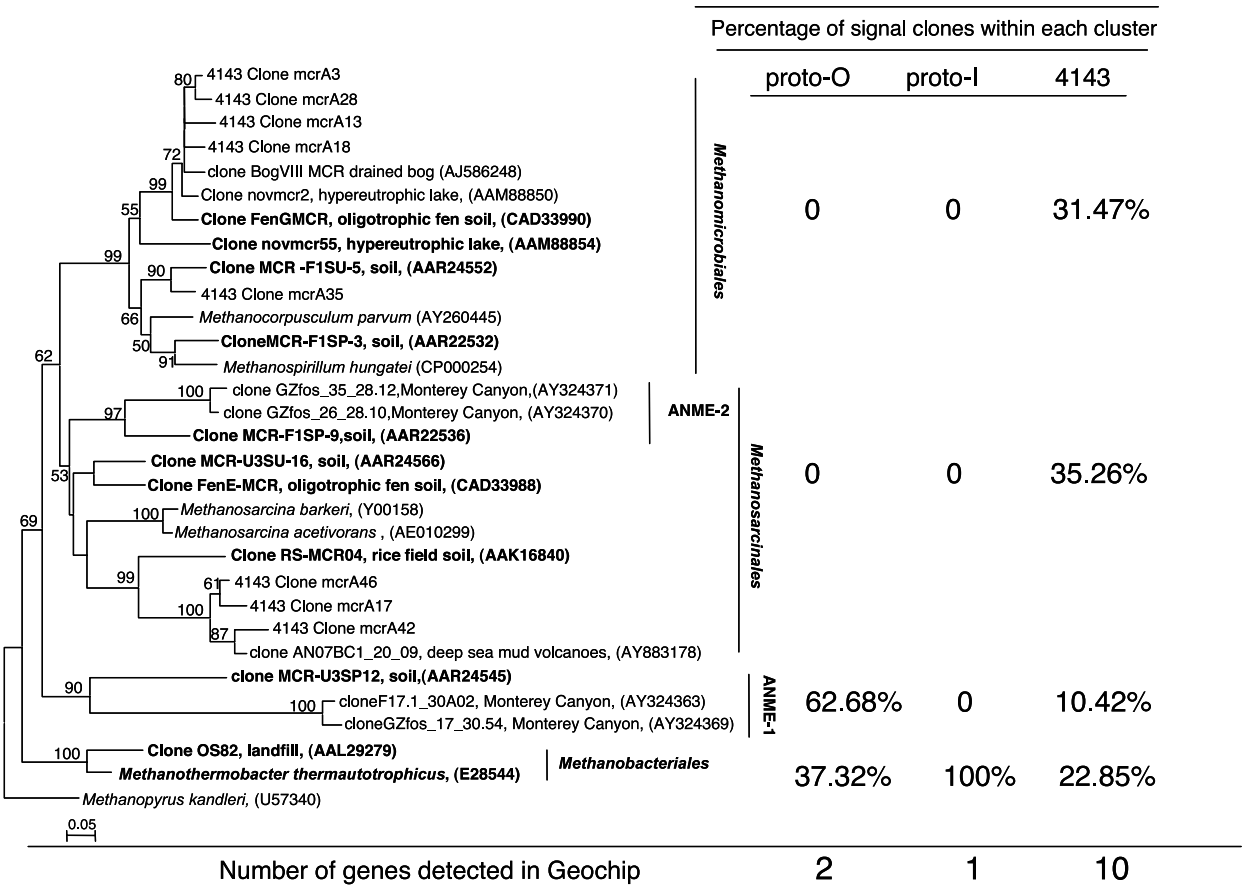

A

Fig. S5. Analysis of *mcrA* and *pmoA* genes detected. (*A*) Phylogenetic tree based on *mcrA* gene sequences. The clones retrieved from 4143-1 through the *mcrA* clone library are designated ''4143-1 Clone *mcrA*,'' followed by the clone number. (*B*) Phylogenetic tree based on *pmoA* gene sequences. Sequences collected from GeoChip hybridization are shown in bold. The tree was inferred by the neighbor-joining method with Mega 4.0. See the Fig. S2*B* legend for details. (*C*) Hierarchical cluster analysis of *mcrA* genes. (*D*) Hierarchical cluster analysis of *pmoA* genes. See Fig. S4*A* legend for details

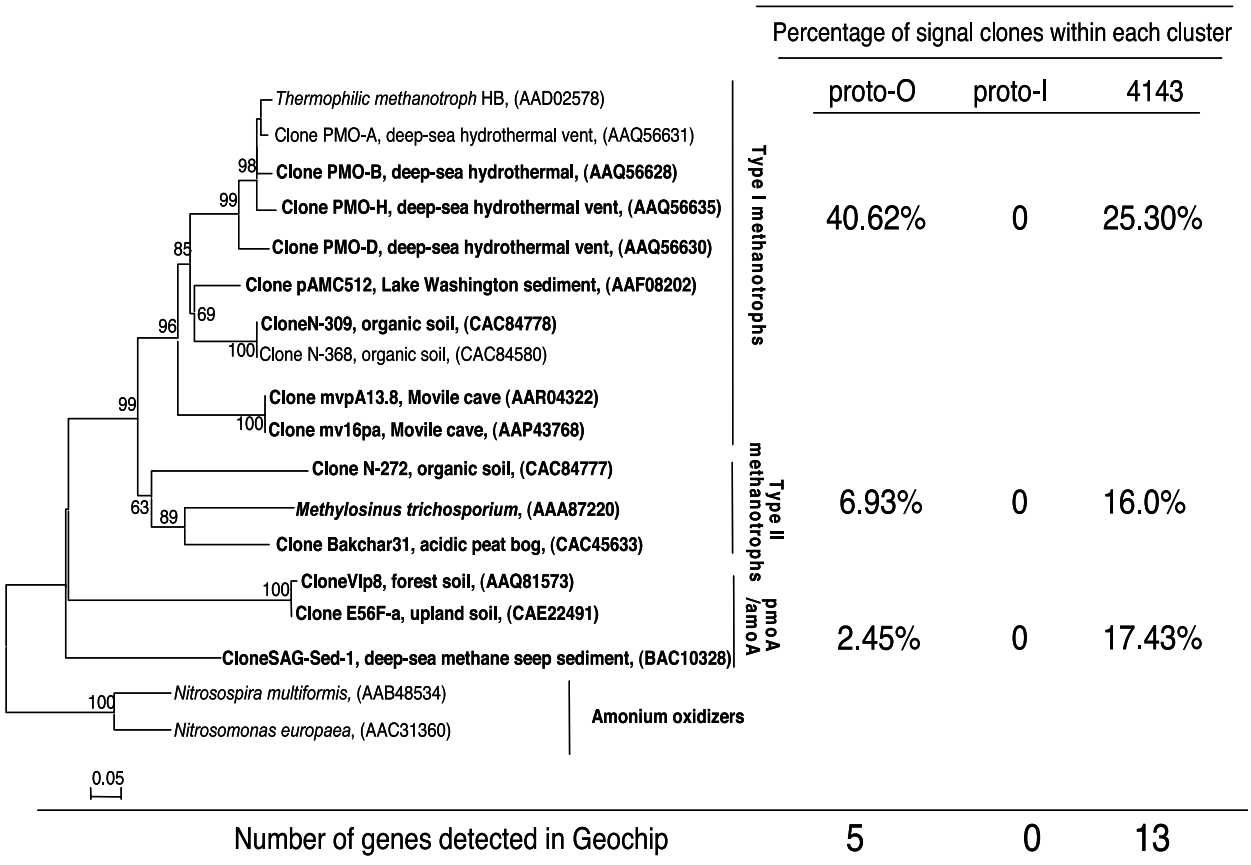

B

Fig. S5. Continued.

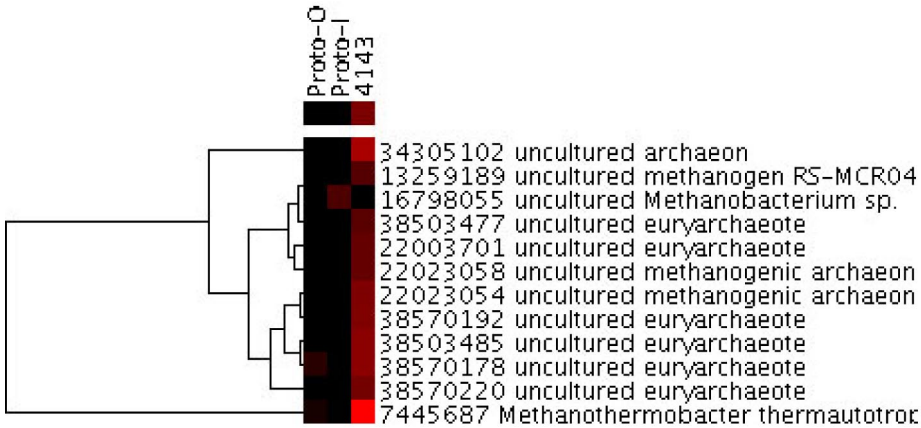

C

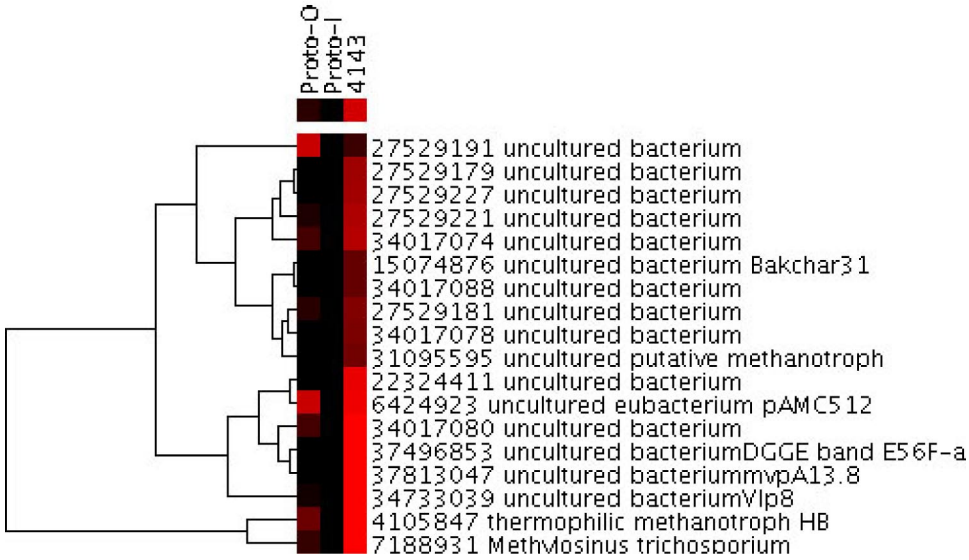

D

Fig. S5. Continued.

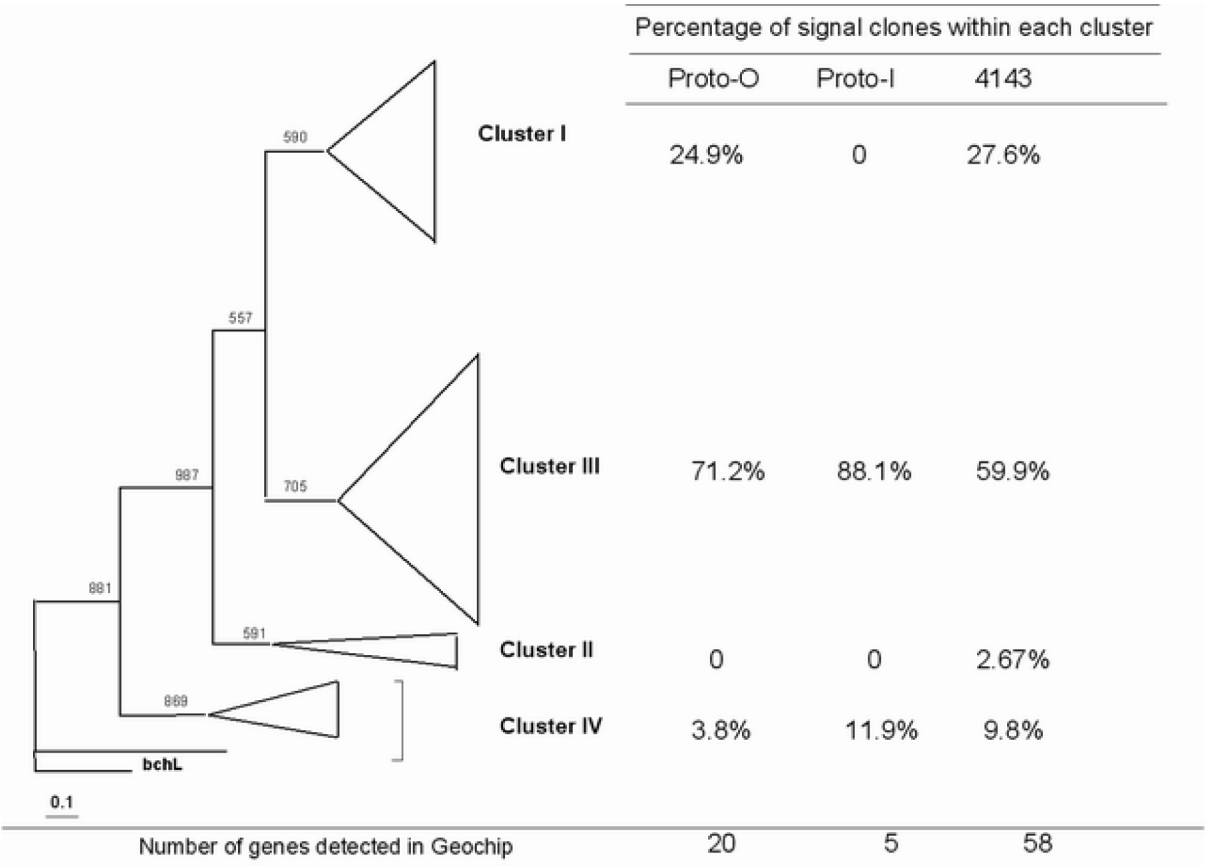

Fig. S6. Maximum-likelihood phylogenetic tree of *nifH* sequences obtained from GeoChip showing the phylogenetic relationship among the 4 *nifH* clusters. The depth and width of each wedge are proportional to the branch lengths and number of *nifH* sequences within each cluster, respectively. Cluster I contains α-, β-, and γ-proteobacterial *nifH* sequences; cluster III contains anaerobic bacterial *nifH* sequences; cluster II contains methanogen and alternative *nifH* sequences; and cluster IV contains divergent archaeal *nifH* sequences. Light-independent protochlorophyllide reductase subunit L gene (*bchL*) from *Chlorobium tepidum* was used as an outgroup. The percentage of signal clones detected in each sample was listed near the phylogenetic tree. The total number of genes detected in GeoChip was summarized.

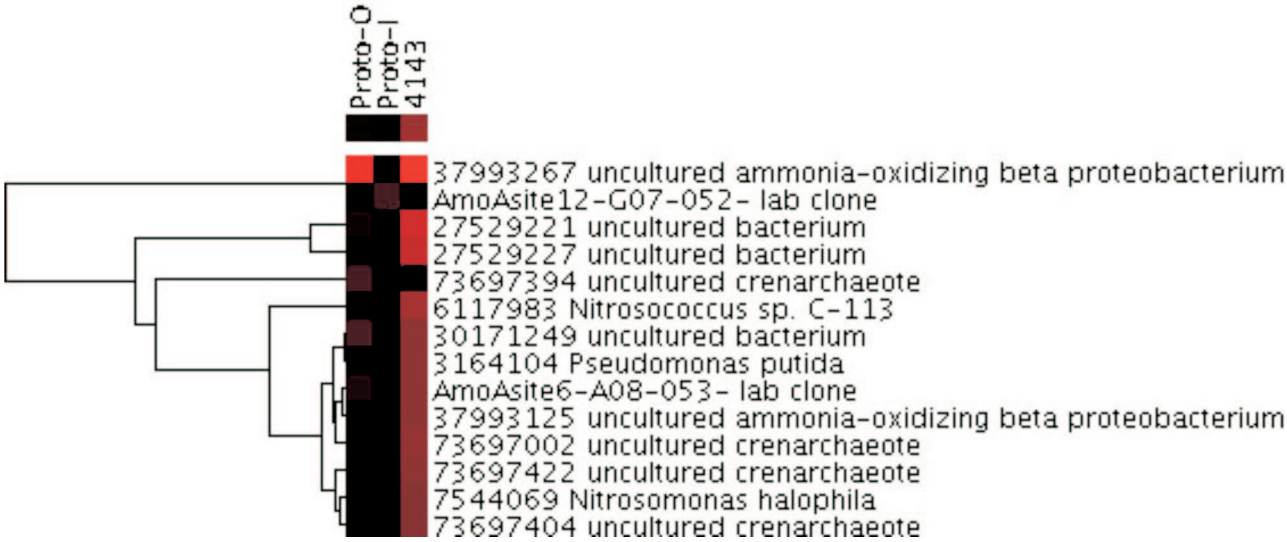

Fig. S7A. Hierarchical cluster analysis of *amoA* genes. See Fig. S4*A* legend for details.

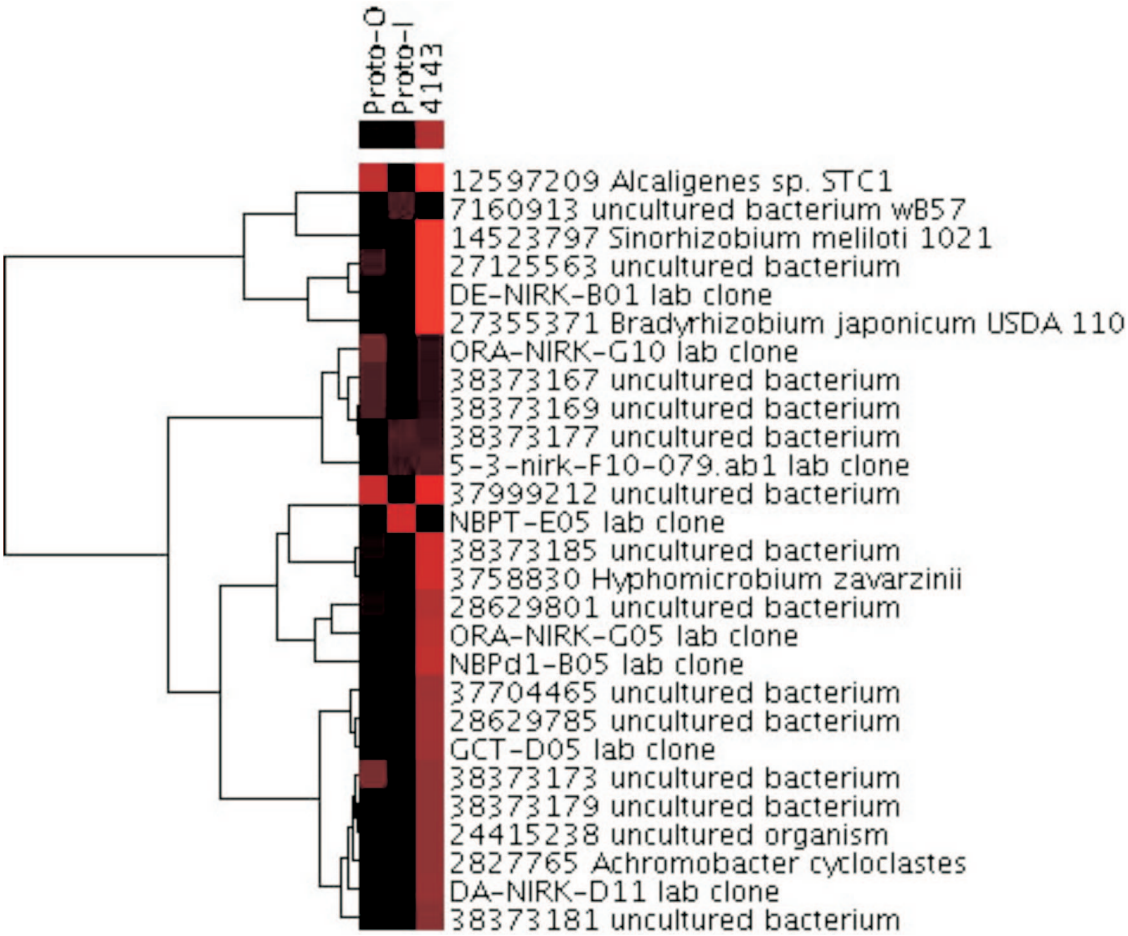

Fig. S7B. Hierarchical cluster analysis of *nirK* genes. See Fig. S4*A* legend for details.

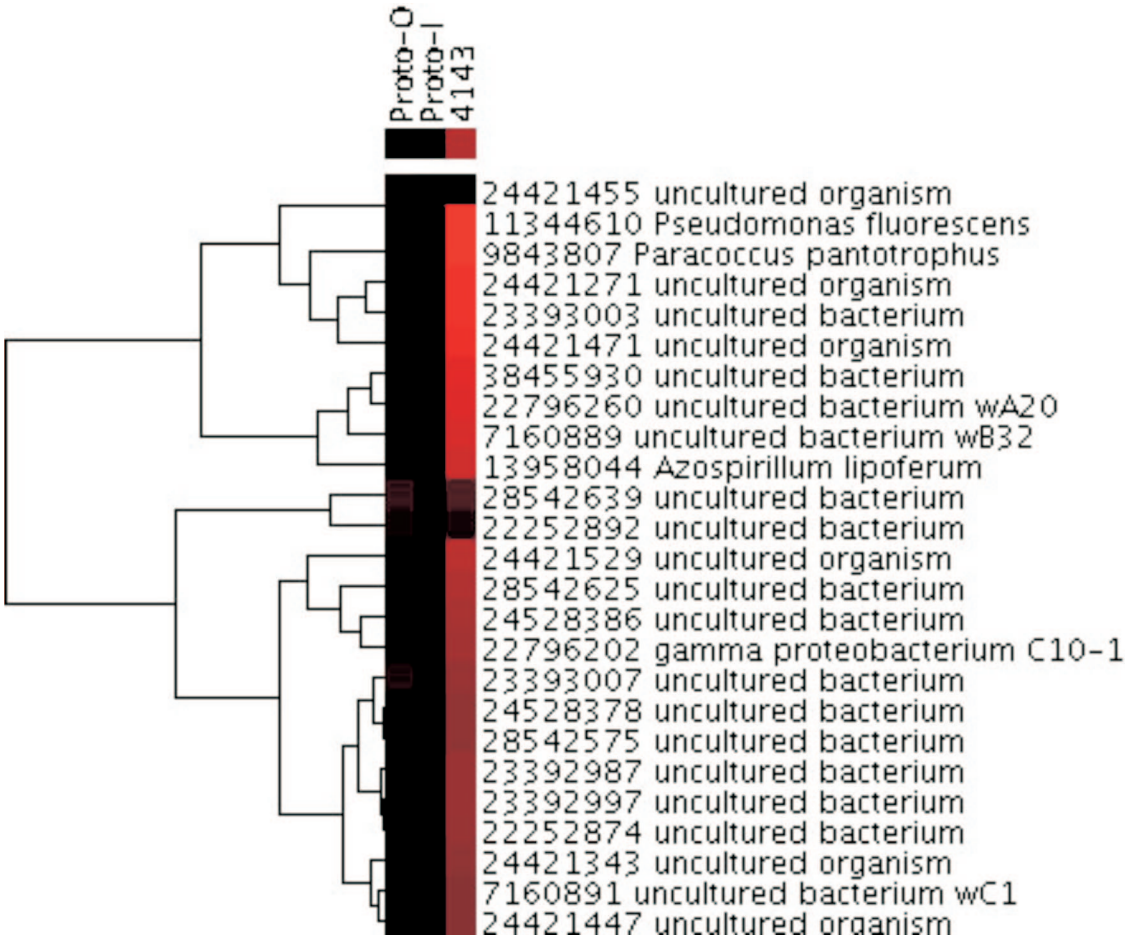

Fig. S7C. Hierarchical cluster analysis of *nirS* genes. See Fig. S4*A* legend for details.

Table S1. Distribution of functional genes detected for major metabolic processes in chimney samples from Juan de Fuca Ridge

	Sample, no. (%)		
Gene category	Proto-I	Proto-O	4143-1
Organic contaminant degradation	53 (46.9)	217 (43.1)	2,008 (37.1)
Carbon degradation	11 (9.7)	56 (11.1)	563 (10.4)
Carbon fixation	6 (5.3)	14 (2.8)	190 (3.5)
Nitrogen fixation	5 (4.4)	22 (4.4)	233 (4.3)
Nitrate reduction	8 (7.1)	30 (6)	534 (9.9)
Nitrification	11 (9.7)	23 (4.6)	391 (7.2)
Methanogenesis	1 (0.9)	2 (0.4)	62 (1.1)
Anaerobic oxidation of methane	0	1 (0.2)	3 (0.1)
Aerobic oxidation of methane	1 (0.9)	14 (2.8)	86 (1.6)
Sulfate reduction	3 (2.7)	28 (5.6)	396 (7.3)
Metal resistance	12 (10.6)	92 (18.3)	910 (16.8)
Total genes	113	504	5,414

Table S2. *rbcL* genes detected by GeoChip

Probe reference no.	Gene	Reference sequence/organism	Signal intensity
Proto-O			
BAC54026	rbcL	Rhodobacter veldkampii	0.2042
AAR21097	rbcL	Thioalkalispira microaerophila	0.357
BAA94444	rbcL	Uncultured deep-sea autotrophic bacterium ORII-2	0.4093
P04718	rbcL	Rhodospirillum rubrum	0.5155
AAR03652	rbcL	Uncultured proteobacterium	0.5576
ZP_00009413	rbcL	Rhodopseudomonas palustris	0.5996
AAR03656	rbcL	Uncultured proteobacterium	0.7224
AAM30945	rbcL	Methanosarcina mazei Go1	0.9123
BAA94433	rbcL	Thiobacillus sp. Lamellibrachia symbiont-2	2.4171
BAA92470	rbcL	Uncultured deep-sea autotrophic bacterium TAGI-2	4.1006
Proto-I			
AAM34461	rbcL	Uncultured deep-sea autotrophic bacterium JTI-1	0.2978
NP_442120	rbcL	Synechocystis sp. PCC 6803	0.3369
NP_662651	rbcL	Uncultured bacterium	0.3664
BAC10575	rbcL	Synechocystis trididemni	1.0053
AAR37722	rbcL	Chlorobium tepidum TLS	1.0612
4143			
BAA92470	rbcL	Uncultured deep-sea autotrophic bacterium TAGI-2	5.8437
BAA92471	rbcL	Uncultured deep-sea autotrophic bacterium TAGI-3	4.0193
BAA94447	rbcL	Uncultured deep-sea autotrophic bacterium ORII-5	2.9827
P04718	rbcL	Rhodospirillum rubrum	2.7958
BAA94440	rbcL	Uncultured deep-sea autotrophic bacterium JTII-4	2.7701
BAA94433	rbcL	Thiobacillus sp. Lamellibrachia symbiont-2	2.5599
ZP_00052722	rbcL	Magnetospirillum magnetotacticum	2.4597
AAC37141	rbcL	Rhodobacter capsulatus	2.4199
ZP_00034564	rbcL	Burkholderia fungorum	2.3454
AAR03656	rbcL	Uncultured proteobacterium	2.2593
AAR21097	rbcL	Thioalkalispira microaerophila	2.216
AAM26289	rbcL	Uncultured bacterium	2.1916
ZP_00009413	rbcL	Rhodopseudomonas palustris	1.9111
AAM30945	rbcL	Methanosarcina mazei Go1	1.8641
BAA94444	rbcL	Uncultured deep-sea autotrophic bacterium ORII-2	1.8121
BAA94449	rbcL	Uncultured deep-sea autotrophic bacterium ORII-7	1.6565
BAC54026	rbcL	Rhodobacter veldkampii	1.6529
BAA92481	rbcL	Uncultured deep-sea autotrophic bacterium OTI-12	1.6344
ZP_00009863	rbcL	Rhodopseudomonas palustris	1.611
AAM34469	rbcL	Uncultured bacterium	1.5313
NP_070416	rbcL	Archaeoglobus fulgidus DSM 4304	1.4807
AAR21099	rbcL	Acidithiobacillus ferrooxidans	1.4524
AAM26291	rbcL	Uncultured bacterium	1.4081
BAA94428	rbcL	Uncultured deep-sea autotrophic bacterium SBII-1	1.3347
BAA94432	rbcL	Uncultured deep-sea autotrophic bacterium SBII-5	1.2621
BAA92469	rbcL	Uncultured deep-sea autotrophic bacterium TAGI-1	1.2023
BAA92490	rbcL	Uncultured deep-sea autotrophic bacterium OTI-4	1.1499
AAM26292	rbcL	Uncultured bacterium	1.1211
AAR03657	rbcL	Uncultured proteobacterium	1.0893
ZP_00011740	rbcL	Rhodopseudomonas palustris	1.0766
NP_682296	rbcL	Thermosynechococcus elongatus BP-1	1.0719
AAR00245	rbcL	Xanthobacter sp. COX	1.0493
BAA94431	rbcL	Uncultured deep-sea autotrophic bacterium SBII-4	1.0112